

Neural Network Matrix Product Operator: A Multi-Dimensionally Integrable Machine Learning Potential

Kentaro Hino*

Department of Chemistry, Graduate School of Science, Kyoto University,
Kitashirakawa Oiwake-cho, Sakyo-ku Kyoto, 606-8502, Japan

Yuki Kurashige†

Department of Chemistry, Graduate School of Science, Kyoto University,
Kitashirakawa Oiwake-cho, Sakyo-ku Kyoto, 606-8502, Japan
FOREST, JST, Honcho 4-1-8, Kawaguchi, Saitama 332-0012, Japan and
CREST, JST, Honcho 4-1-8, Kawaguchi, Saitama 332-0012, Japan

(Dated: November 4, 2024)

A neural network-based machine learning potential energy surface (PES) expressed in a matrix product operator (NN-MPO) is proposed. The MPO form enables efficient evaluation of high-dimensional integrals that arise in solving the time-dependent and time-independent Schrödinger equation, and effectively overcomes the so-called curse of dimensionality. This starkly contrasts with other neural network-based machine learning PES methods, such as multi-layer perceptrons (MLPs), where evaluating high-dimensional integrals is not straightforward due to the fully connected topology in their backbone architecture. Nevertheless, the NN-MPO retains the high representational capacity of neural networks. NN-MPO can achieve spectroscopic accuracy with a test mean absolute error (MAE) of 3.03 cm^{-1} for a fully coupled six-dimensional *ab initio* PES, using only 625 training points distributed across a 0 to $17,000 \text{ cm}^{-1}$ energy range. Our Python implementation is available at <https://github.com/KenHino/Pompon>.

I. INTRODUCTION

The developments of machine learning potential energy surfaces (PESs) in quantum chemistry and condensed matter physics have been accelerating alongside the advancements in a wide range of computational technologies [1–6]. Neural network potentials, in particular, have garnered significant attention for their ability to reproduce the accurate but expensive *ab initio* electronic structure calculations. For universal interatomic potentials, the model input is often replaced by user-defined descriptors that are augmented with atomic numbers and symmetry-consistent features, such as interatomic distances [7–11]. The incorporation of atomic descriptors enables the model to estimate individual atomic energies. Consequently, by summing these atomic contributions, the model can predict the total potential energy of systems comprising arbitrary numbers of atoms.

Neural network potentials commonly employ multi-layer perceptrons (MLPs) as their foundational architecture. These structures are characterized by their extensive parameter spaces, which allow them to approximate highly complex functions. Notably, despite the substantial number of parameters involved, recent research has demonstrated that overparameterized neural networks, when trained using stochastic optimization techniques, exhibit the ability to mitigate complexity-induced errors and achieve robust generalization performance [12–14].

Trained neural network potentials can predict properties without computationally expensive *ab initio* calculations. In particular, using neural network potential as a force field for classical molecular dynamics simulation that treats the nuclear motions as classical particles is becoming a promising approach [15, 16].

On the other hand, in the context of quantum many-body simulations, if we consider replacing the potential \hat{V} of Hamiltonians with a machine learning potential $V(\mathbf{x})$,

$$\hat{H} = \hat{T} + \hat{V} = - \sum_{i=1}^n \frac{\hbar^2}{2M_i} \nabla_i^2 + V(\mathbf{x}), \quad (1)$$

one of the bottlenecks lies in the evaluation of the multi-dimensional integrals between wavefunction Ψ and Hamiltonian \hat{H} , which appears not only in the evaluation of the expectation value $\langle \Psi | \hat{H} | \Psi \rangle$ but also in the updating procedures of variational parameters based on the variational principle $\langle \delta \Psi | \hat{H} | \Psi \rangle$, which is repeatedly called in both time-dependent and time-independent problems. Because of the fully connected topology of MLPs, they cannot efficiently evaluate multi-dimensional integrals and often resort to an approximated method such as Monte Carlo integration. Therefore, it is not efficient for nuclear wavepacket simulation such as multi-dimensional time-dependent Hartree (MCTDH) [17, 18], and instead, the sum-of-products (SOP) forms [19–26]

$$V_{\text{SOP}}(\mathbf{x}) = \sum_{\rho} c_{\rho} \prod_i^n v_{\rho_i}(x_i) \quad (2)$$

like polynomials or high-dimensional model representations (HDMR) [27, 28], which approximate an n -body

* hino@theoc.kuchem.kyoto-u.ac.jp

† kura@kuchem.kyoto-u.ac.jp

function as a sum of up to k -body functions,

$$V_{\text{HDMR}}(\mathbf{x}) = \sum_{i_1}^n c_{i_1} v_{i_1}(x_{i_1}) + \sum_{i_1 < i_2}^n c_{i_1 i_2} v_{i_1 i_2}(x_{i_1}, x_{i_2}) + \dots \quad (3)$$

have been employed because both can evaluate multi-dimensional integrals between wavefunction $|\sigma_1\rangle|\sigma_2\rangle\cdots|\sigma_f\rangle$ by the sum of products of one-dimensional integrals $\langle\sigma'_i|v_{\rho_i}|\sigma_i\rangle$ and the sum of k -dimensional integrals $\langle\sigma'_{i_1}\sigma'_{i_2}\cdots\sigma'_{i_k}|v_{i_1 i_2 \dots i_k}|\sigma_{i_1}\sigma_{i_2}\cdots\sigma_{i_k}\rangle$, respectively.

Here, we present a machine learning potential facilitated by tensor network (TN), which offers both high representational power as MLPs and efficient evaluation of multi-dimensional integrals as SOPs and HDMRs. TNs have been initially developed for quantum many-body problems. In particular, the density matrix renormalization group (DMRG) [29, 30] is the most well-known ansatz, established as a method approaching exact solutions in various quantum many-body systems, such as spin systems [29, 30], electronic systems [31, 32], and phonon systems [33]. The matrix product state (MPS) is known as a representation of the many-body wavefunction in a one-dimensional TN called tensor train (TT). This formalism efficiently expresses the exponentially large tensor $A_{i_1 i_2 \dots i_n} \in \mathbb{K}^{d_1 \times d_2 \times \dots \times d_n}$ as a one-dimensional contraction of polynomially-sized three-rank tensors $\{G_{\alpha_{i-1} i \alpha_i}^{[i]} \in \mathbb{K}^{D_{i-1} \times d_i \times D_i}\}$;

$$A_{i_1 i_2 \dots i_n} \approx \sum_{\alpha_1 \alpha_2 \dots \alpha_{n-1}} G_{i_1 \alpha_1}^{[1]} G_{\alpha_1 i_2 \alpha_2}^{[2]} G_{\alpha_2 i_3 \alpha_3}^{[3]} \cdots G_{\alpha_{n-1} i_n}^{[n]}.$$

Because TNs can reproduce the original exponentially large tensor product coefficients $A_{i_1 i_2 \dots i_n}$ in the limit of $\{D_i\}$. *i. e.* rank of connecting indices $\{\alpha_i\}$, TNs should be able to represent any function for machine learning tasks with the desired accuracy. Furthermore, TNs can extract important features from multi-dimensional data through low-rank approximations, which is key to reducing parameters and preventing overfitting in machine learning. *Schwab* and *Stoudenmire* leveraged these properties of TNs. They applied the TT model to the handwritten digit classification task, demonstrating the impressive capabilities [34]. In addition to the affinity of TNs for machine learning tasks, TNs have a unique architecture that enables efficient evaluation of multi-dimensional integrals. The key to this efficiency is the commutative contractions of TNs, which allow the evaluation of multi-dimensional integrals with the sum and product operation of polynomially-sized tensors. In contrast, MLPs present significant challenges for multi-dimensional integral calculations because their fully connected architecture and nonlinear activation functions prevent the application of commutative contractions during forward propagation.

For the evaluation of the integral between wavefunctions and operators written in TNs, the matrix product operator (MPO) [35] form has been introduced, which is a

TT format operator representation and enables the evaluation of the integral in polynomial time provided that the wavefunction is represented by MPS or expanded by a polynomial number of configurations. In this study, TT machine learning model convertible to MPO was applied to predict molecular PES. We also demonstrated its efficiency for many-body quantum simulations through phonon DMRG calculations integrated with the trained TT model.

II. METHODS

A. Model Architecture

In this paper, the dataset

$$\mathcal{D} = \left\{ \left(\mathbf{x}^{(k)}, V^{(k)}, \mathbf{F}^{(k)} \right) \mid k = 1, 2, \dots, |\mathcal{D}| \right\} \quad (4)$$

contains $|\mathcal{D}|$ molecular mass-weighted coordinates $\mathbf{x}^{(k)} \in \mathbb{R}^{1 \times n}$ (row-vector) and corresponding potential energies $V(\mathbf{x}^{(k)}) \in \mathbb{R}$ and analytical forces $\mathbf{F}(\mathbf{x}^{(k)}) = -\frac{\partial V(\mathbf{x}^{(k)})}{\partial \mathbf{x}} \in \mathbb{R}^{1 \times n}$ where n is the number of degrees of freedom of nuclear motion. The batch index (k) is omitted in the following description for simplicity. We designate our model a neural network matrix product operator (NN-MPO), which is represented by the following equation:

$$V_{\text{NN-MPO}}(\mathbf{x}) = \Phi(\mathbf{q})\mathbf{W} \quad (5)$$

$$\mathbf{q} = \mathbf{x}U \quad (6)$$

where $U \in \text{St}(f, n) = \{U \in \mathbb{R}^{n \times f} \mid U^\top U = I_f\}$ is the orthogonal linear transformation matrix that maps the input mass-weighted coordinates \mathbf{x} to the latent space coordinates $\mathbf{q} \in \mathbb{R}^{1 \times f}$:

$$[q_1 \ q_2 \ \cdots \ q_f] = [x_1 \ x_2 \ \cdots \ x_n]U. \quad (7)$$

We refer to U as *Coordinator*. Eq. (5) can be interpreted as a sort of kernel method, where Φ serves as a design matrix and \mathbf{W} as kernel weights. $\Phi(\mathbf{q})$ is represented by tensor product basis:

$$\Phi_{\rho_1 \rho_2 \dots \rho_f} = \{\phi_{\rho_1}^{[1]}(q_1)\} \otimes \{\phi_{\rho_2}^{[2]}(q_2)\} \otimes \cdots \otimes \{\phi_{\rho_f}^{[f]}(q_f)\}. \quad (8)$$

Let the number of basis functions for every degree of freedom be N , *i. e.* ρ_i takes values $1, 2, \dots, N$, resulting in a total number of expanded basis N^f . The model can achieve high representational power by increasing N to a sufficiently large value. For simplicity, we rewrite the basis function $\phi_{\rho_i}^{[i]}(q_i)$ as ϕ_{ρ_i} . The choice of the basis function ϕ_{ρ_i} is crucial for the performance. In the previous study for the handwritten digit classification [34], the authors employed $\phi_{\rho_i}(x_i) = [\cos(\frac{\pi}{2}x_i), \sin(\frac{\pi}{2}x_i)]$ for the pixel value x_i . However, this choice is not suitable for the molecular PES. For instance, *Baranov* and *Oseledets* demonstrated the TT-based PES [36] using

ϕ_{ρ_i} as Chebyshev polynomial, trained through the combination of tensor cross interpolation [37, 38] and Chebyshev approximation, which is an interpolation method for Chebyshev nodes. Chebyshev nodes are automatically determined once the input interval and the polynomial order are given. On the other hand, NN-MPO can be trained through gradient-based optimization, which does not limit the number of training data points. Therefore, we can sample the training data points from the physically reasonable distribution. Based on the strong prior knowledge of the PES structure, we chose the following basis function:

$$\phi_{\rho_i}(q_i) = \begin{cases} 1 & \text{for } \rho_i = 1 \\ 1 - \exp\left(-\left(q_{\rho_i}^{(i)}\right)^2\right) + \epsilon \left(q_{\rho_i}^{(i)}\right)^2 & \text{for } 2 \leq \rho_i \leq \lceil \frac{N}{2} \rceil \\ \frac{q_{\rho_i}^{(i)}}{1 + \exp\left(-q_{\rho_i}^{(i)}\right)} & \text{for } \lceil \frac{N}{2} \rceil < \rho_i \leq N \end{cases} \quad (9)$$

where

$$q_{\rho_i}^{(i)} = w_{\rho_i}^{(i)} \left(q_i - \bar{q}_{\rho_i}^{(i)} \right) + b_{\rho_i}^{(i)} \quad (10)$$

and $\bar{q}_{\rho_i}^{(i)} = \sum_j \bar{x}_{\rho_i}^{(j)} U_{ji}$. We randomly chose reference positions $\bar{x}_{\rho_i}^{(j)}$ from the training data. It could be seemed that $\bar{q}_{\rho_i}^{(i)}$ is redundant, $-w_{\rho_i}^{(i)} \bar{q}_{\rho_i}^{(i)}$ is absorbed into $b_{\rho_i}^{(i)}$, however, finding initial $b_{\rho_i}^{(i)}$ stable to the change of coordinator U is difficult. Therefore, like a kernel method, we chose reference positions $\bar{x}_{\rho_i}^{(j)}$ from training data in advance and initialized $b_{\rho_i}^{(i)} = 0$. Besides \mathbf{W} , the traing parameters are U , $w_{\rho_i}^{(i)}$, and $b_{\rho_i}^{(i)}$. In Eq. (9), the first activation function is nothing other than a constant function, which is inspired by the idea of HDMR: n -body function can be approximated by the sum of up to k -body functions, which $n - k$ variables of them are constant. The second one, $1 - \exp(-x^2) + \epsilon x^2$, was introduced by *Koch et al* to the SOP neural network in the application to the excited state PES of H_2CO molecule [23], which is similar to a Gaussian function but moderately increases the quadratic term and may probably be suitable for the vibrational PES because it prohibits the unphysical holes in the PES. We set $\epsilon = 0.05$, the same as the previous work. The third one, $\frac{x}{1 + \exp(-x)}$, is known as *silu* or *swish* function [39], a sophisticated activation function in a deep learning community, and we realized that this function is similar to Morse potential or Lennard-Jones potential, which may probably be suitable for the description of the dissociation limit.

Once the basis function Φ is defined, the weight \mathbf{W} can be optimized. While the size of \mathbf{W} can naively reach N^f , we can reduce the number of parameters by using the TT structure:

$$\mathbf{W} = \mathbf{W}^{(1)} \mathbf{W}^{(2)} \dots \mathbf{W}^{(f)} \quad (11)$$

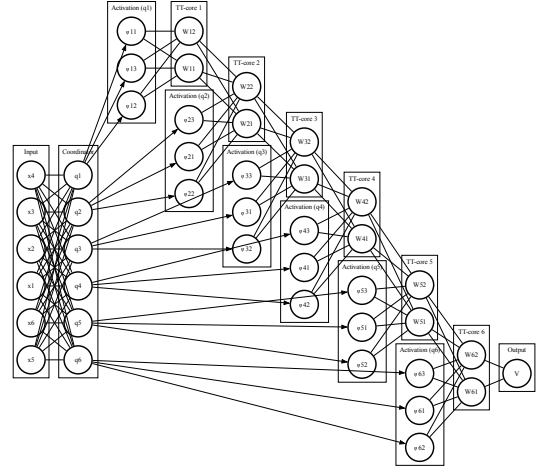


FIG. 1. The conventional diagram in the deep learning community. This diagram indicates NN-MPO for $n = f = 6$, $N = 3$, and $M = 2$.

in other form,

$$W_{\rho_1 \rho_2 \dots \rho_f} = \sum_{\beta_1 \beta_2 \dots \beta_{f-1}} W_{1\beta_1}^{\rho_1} W_{\beta_1 \beta_2}^{\rho_2} \dots W_{\beta_{f-1} 1}^{\rho_f} \quad (12)$$

where each “core” tensor $W_{\beta_{i-1} \beta_i}^{\rho_i} \in \mathbb{R}^{M_{i-1} \times N \times M_i}$ can achieve the low-rank approximation, which enables not only the reduction of parameter but also the mitigation of complexity errors such as overfitting. The connecting index β takes $\beta = 1, 2, \dots, M$ where M is called bond dimension, link dimension, or TT-rank. The following equations write the full formulation of NN-MPO:

$$\begin{aligned} V_{\text{NN-MPO}}(\mathbf{x}) &= \tilde{V}_{\text{NN-MPO}}(\mathbf{q}) \\ &= \sum_{\substack{\rho_1, \rho_2, \dots, \rho_f \\ \beta_1, \beta_2, \dots, \beta_{f-1}}} \phi_{\rho_1}(q_1) \dots \phi_{\rho_f}(q_f) W_{1\beta_1}^{\rho_1} W_{\beta_1 \beta_2}^{\rho_2} \dots W_{\beta_{f-1} 1}^{\rho_f}. \end{aligned} \quad (13)$$

The corresponding diagrams of the architecture are shown in Fig. 1 and Fig. 2.

B. Optimization

We defined the loss function \mathcal{L} as a sum of energy and force mean squared errors (MSE).

$$\mathcal{L} = \mathcal{L}_{\text{energy}} + \mathcal{L}_{\text{force}} \quad (14)$$

$$\mathcal{L}_{\text{energy}} = \frac{1}{|\mathcal{D}|} \sum_{\mathbf{x}, V \in \mathcal{D}} \frac{1}{2} \|V_{\text{NN-MPO}}(\mathbf{x}) - V\|^2 \quad (15)$$

$$\mathcal{L}_{\text{force}} = \frac{1}{|\mathcal{D}|} \sum_{\mathbf{x}, \mathbf{F} \in \mathcal{D}} \frac{1}{2} \left\| -\frac{\partial V_{\text{NN-MPO}}(\mathbf{x})}{\partial \mathbf{x}} - \mathbf{F} \right\|^2 \quad (16)$$

$$= \frac{1}{|\mathcal{D}|} \sum_{\mathbf{x}, \mathbf{F} \in \mathcal{D}} \frac{1}{2} \left\| -\frac{\partial \tilde{V}_{\text{NN-MPO}}(\mathbf{q})}{\partial \mathbf{q}} - \mathbf{F} U \right\|^2 \quad (17)$$

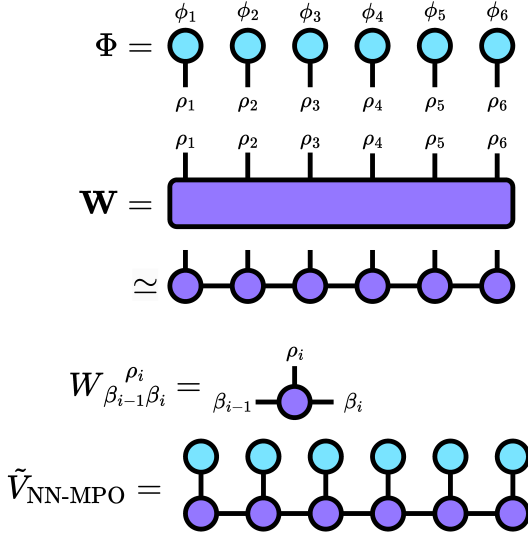


FIG. 2. The conventional diagram in the tensor network community. This diagram indicates NN-MPO for $f = 6$. Coordinator layer is omitted.

The gradient of $w_{\rho_i}^{(i)}, b_{\rho_i}^{(i)}$ and U to the loss function \mathcal{L} can be evaluated by the automatic differentiation facilitated by the deep learning framework. In our implementation, JAX library was used [40]. These parameters were updated by the Adam optimization[41]. In addition, we used QR decomposition to retract U onto the Stiefel manifold to keep the orthogonality for each step [42, 43]. We referred to the implementation of the Riemannian Adam optimization algorithm in `geoopt` library [44].

The optimization scheme of TT core tensor $W_{\beta_{i-1}\beta_i}^{\rho_i}$ is different from the conventional neural network optimization because TN has gauge freedom, which means that TN can return the same value from the contraction of different tensors, for instance, $A_{ij} = \sum_k U_{ik} \Sigma_{kk} V_{kj} = \sum_k U_{ik} C_{kj} = \sum_k D_{ik} V_{kj}$. The DMRG algorithm successfully imposed the canonical gauge form on the MPS and updated each core tensor from left to right and right to left (a strategy called *sweeping*). We employed the same approach for the TT core optimization. It is helpful to introduce the following gauge fixed notation:

$$B_{\beta_{i-1}\beta_{i+1}}^{\rho_i\rho_{i+1}} := \sum_{\beta_i} W_{\beta_{i-1}\beta_i}^{\rho_i} W_{\beta_i\beta_{i+1}}^{\rho_{i+1}} \quad (18)$$

$$= \sum_{\beta_i} U_{\beta_{i-1}\beta_i}^{\rho_i} \Sigma_{\beta_i}^{\rho_i} V_{\beta_i\beta_{i+1}}^{\rho_{i+1}} \quad (19)$$

$$= \sum_{\beta_i} U_{\beta_{i-1}\beta_i}^{\rho_i} C_{\beta_i\beta_{i+1}}^{\rho_{i+1}} \quad (20)$$

$$= \sum_{\beta_i} C_{\beta_{i-1}\beta_i}^{\rho_i} V_{\beta_i\beta_{i+1}}^{\rho_{i+1}}. \quad (21)$$

Eq (19) is the singular value decomposition (SVD) of the matrix with row $\rho_i \otimes \beta_{i-1}$ and column $\rho_{i+1} \otimes \beta_{i+1}$. The diagram corresponding to these equations is shown in Fig. 3. By repeating the SVD of the TT core tensor,

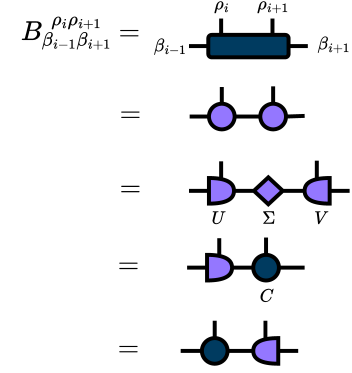


FIG. 3. The diagram of two-dots and one-dot center core in TT, both of which are filled with navy color.

The following gauge-fixed equation rewrites TT:

$$\begin{aligned} & \sum_{\beta_1 \cdots \beta_{f-1}} W_{1\beta_1}^{\rho_1} W_{\beta_1\beta_2}^{\rho_2} \cdots W_{\beta_{f-1}1}^{\rho_f} \\ &= \sum_{\beta_1 \cdots \beta_{f-1}} C_{1\beta_1}^{\rho_1} V_{\beta_1\beta_2}^{\rho_2} \cdots V_{\beta_{f-1}1}^{\rho_f} \\ &= \sum_{\beta_2 \cdots \beta_{f-1}} B_{1\beta_2}^{\rho_1\rho_2} V_{\beta_2\beta_3}^{\rho_3} \cdots V_{\beta_{f-1}1}^{\rho_f} \quad (22) \\ &= \sum_{\beta_1 \cdots \beta_{f-1}} U_{1\beta_1}^{\rho_1} C_{\beta_1\beta_2}^{\rho_2} V_{\beta_2\beta_3}^{\rho_3} \cdots V_{\beta_{f-1}1}^{\rho_f} \\ &\vdots \end{aligned}$$

Then, we can minimize the loss function \mathcal{L} to $B_{\beta_{i-1}\beta_{i+1}}^{\rho_i\rho_{i+1}}$ (as well as $C_{\beta_{i-1}\beta_i}^{\rho_i}$). The force loss function $\mathcal{L}_{\text{force}}$ can be further simplified. The predicted force in Eq (17) is $-\frac{\partial \tilde{V}_{\text{NN-MPO}}(\mathbf{q})}{\partial \mathbf{q}} = \mathbf{W} \left(-\frac{\partial \Phi(\mathbf{q})}{\partial \mathbf{q}} \right)$ where

$$\begin{aligned} & -\frac{\partial \Phi(\mathbf{q})}{\partial \mathbf{q}} \\ &= \left[-\frac{\partial \Phi(\mathbf{q})}{\partial q_1} \quad -\frac{\partial \Phi(\mathbf{q})}{\partial q_2} \quad \cdots \quad -\frac{\partial \Phi(\mathbf{q})}{\partial q_f} \right] \\ &= \left[\begin{array}{cccc} \left\{ -\frac{\partial \phi_{\rho_1}}{\partial q_1} \right\} & \otimes & \{ \phi_{\rho_2} \} & \otimes \cdots \otimes \{ \phi_{\rho_f} \} \\ \{ \phi_{\rho_1} \} & \otimes & \left\{ -\frac{\partial \phi_{\rho_2}}{\partial q_2} \right\} & \otimes \cdots \otimes \{ \phi_{\rho_f} \} \\ & & \vdots & \\ \{ \phi_{\rho_1} \} & \otimes & \{ \phi_{\rho_2} \} & \otimes \cdots \otimes \left\{ -\frac{\partial \phi_{\rho_f}}{\partial q_f} \right\} \end{array} \right]^{\top}. \quad (23) \end{aligned}$$

To simplify the loss function, we redefine the database \mathcal{D}' which contains $|\mathcal{D}'| = |\mathcal{D}| \times (f+1)$ data. The index of the data point is redefined as

$$\{p\} := \{k\} \otimes \{r\} \quad (24)$$

where $k = 1, 2, \dots, |\mathcal{D}|$ is the index of the original data point and $r = 1, 2, \dots, f+1$ is the index of the concatenated array of \mathbf{F} and V . The input and output set is

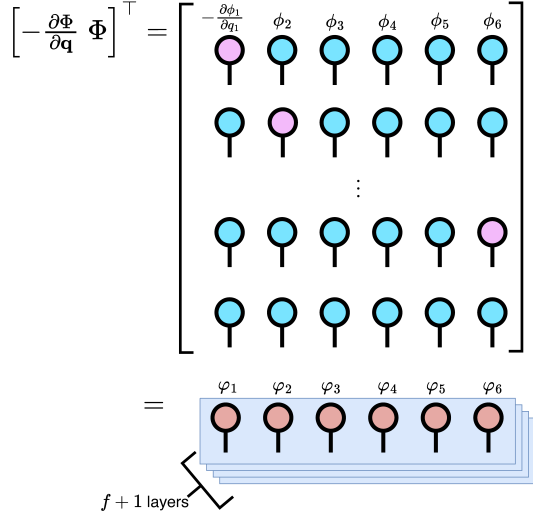


FIG. 4. The diagram of basis concatenated force and energy.

redefined as

$$\varphi_{\rho_i}^p := \bar{\varphi}_{r\rho_i}^{(k)} := \begin{cases} -\frac{\partial \phi_{\rho_i}(q_i^{(k)})}{\partial q_i} & \text{for } r = i \\ \phi_{\rho_i}(q_i^{(k)}) & \text{otherwise} \end{cases} \quad (25)$$

$$y_p := \bar{y}_r^{(k)} := \begin{cases} \sum_i \mathbf{F}_i^{(k)} U_{ir} & \text{for } 1 \leq r \leq f \\ V^{(k)} & \text{for } r = f + 1 \end{cases} \quad (26)$$

Furthermore, we introduce the following notation:

$$\Phi_{p\beta_{i-1}}^{[i-1]} := \sum_{\substack{\rho_1 \cdots \rho_{i-1} \\ \beta_1 \cdots \beta_{i-2}}} U_{1\beta_1}^{\rho_1} \cdots U_{\beta_{i-2}\beta_{i-1}}^{\rho_{i-1}} \varphi_{\rho_1}^p \cdots \varphi_{\rho_{i-1}}^p \quad (27)$$

$$\Phi_{p\beta_{i+1}}^{[i+2]} := \sum_{\substack{\rho_{i+2} \cdots \rho_f \\ \beta_{i+2} \cdots \beta_{f-1}}} V_{\beta_{i+1}\beta_{i+2}}^{\rho_{i+2}} \cdots V_{\beta_{f-1}\beta_f}^{\rho_f} \varphi_{\rho_{i+2}}^p \cdots \varphi_{\rho_f}^p \quad (28)$$

$$\Phi_{\beta_{i-1}\beta_{i+1}}^{\rho_i \rho_{i+1}} := \Phi_{p\beta_{i-1}}^{[i-1]} \varphi_{\rho_i}^p \varphi_{\rho_{i+1}}^p \Phi_{p\beta_{i+1}}^{[i+2]} \quad (29)$$

Then, the total loss function becomes

$$\mathcal{L} = \frac{1}{|\mathcal{D}'|} \sum_p \bar{\mathcal{L}} \left(B_{\beta_{i-1}\beta_{i+1}}^{\rho_i \rho_{i+1}}; \Phi_{\beta_{i-1}\beta_{i+1}}^{\rho_i \rho_{i+1}}, y_p \right) \quad (30)$$

where

$$\begin{aligned} & \bar{\mathcal{L}} \left(B_{\beta_{i-1}\beta_{i+1}}^{\rho_i \rho_{i+1}}; \Phi_{\beta_{i-1}\beta_{i+1}}^{\rho_i \rho_{i+1}}, y_p \right) \\ &= \frac{1}{2} \left\| \sum_{\substack{\rho_i \rho_{i+1} \\ \beta_{i-1}\beta_{i+1}}} \Phi_{\beta_{i-1}\beta_{i+1}}^{\rho_i \rho_{i+1}} B_{\beta_{i-1}\beta_{i+1}}^{\rho_i \rho_{i+1}} - y_p \right\|^2. \end{aligned} \quad (31)$$

We can minimize Eq. (30) in either two ways. One way is to use the analytical gradient of $B_{\beta_{i-1}\beta_{i+1}}^{\rho_i \rho_{i+1}}$:

$$\frac{\partial \bar{\mathcal{L}}}{\partial B} = \left(\sum_{\substack{\rho_i \rho_{i+1} \\ \beta_{i-1}\beta_{i+1}}} \Phi_{\beta_{i-1}\beta_{i+1}}^{\rho_i \rho_{i+1}} B_{\beta_{i-1}\beta_{i+1}}^{\rho_i \rho_{i+1}} - y_p \right) \Phi_{\beta_{i-1}\beta_{i+1}}^{\rho_i \rho_{i+1}} \quad (32)$$

and update $B_{\beta_{i-1}\beta_{i+1}}^{\rho_i \rho_{i+1}}$ by the gradient-based optimization algorithm such as Adam. This approach is suitable when the batch size $|\mathcal{D}'|$ and the number of parameters $M^2 N^2$ are significant or gradual changes of TT required.

The other way is regarding the minimization problem as a quadratic form problem which minimizes the following function:

$$f(\mathbf{x}) = \frac{1}{2} \mathbf{x}^\top A \mathbf{x} - \mathbf{x}^\top b \quad (33)$$

where \mathbf{x} is the vectorized $B_{\beta_{i-1}\beta_{i+1}}^{\rho_i \rho_{i+1}}$, Hessian matrix $A = \sum_p \left(\Phi_{\beta_{i-1}\beta_{i+1}}^{\rho_i \rho_{i+1}} \right)^\top \Phi_{\beta_{i-1}\beta_{i+1}}^{\rho_i \rho_{i+1}}$ and $b = \sum_p \left(\Phi_{\beta_{i-1}\beta_{i+1}}^{\rho_i \rho_{i+1}} \right)^\top y_p$. This problem is solved by the conjugate gradient (CG) method, without explicitly storing the Hessian matrix $A \in \mathbb{R}^{M^2 N^2 \times M^2 N^2}$ and $\Phi_{\beta_{i-1}\beta_{i+1}}^{\rho_i \rho_{i+1}} \in \mathbb{R}^{|\mathcal{D}'| \times N \times N \times M \times M}$, both of which are constructed from $\Phi_{p\beta_{i-1}}^{[i-1]}$, $\Phi_{p\beta_{i+1}}^{[i+2]}$, $\varphi_{\rho_i}^p$ and $\varphi_{\rho_{i+1}}^p$. The algorithm is shown in Algorithm 1. This approach is suitable when the batch size $|\mathcal{D}'|$ and the number of parameters $M^2 N^2$ are small and rapid convergence to the fixed basis function is required.

Once the TT core tensor $B_{\beta_{i-1}\beta_{i+1}}^{\rho_i \rho_{i+1}}$ is optimized, SVD is executed to truncate the bond dimension to M . Then, the center core tensor is swept to the neighboring core by gauge transformation in Eq. (18), and repeat these procedures until the optimal value is obtained. In addition, by replacing $B_{\beta_{i-1}\beta_{i+1}}^{\rho_i \rho_{i+1}}$ with $C_{\beta_{i-1}\beta_i}^{\rho_i}$ and $\Phi_{p\beta_{i+1}}^{[i+2]}$ with $\Phi_{p\beta_i}^{[i+1]} = \sum_{\beta_{i+1}}^{\rho_{i+1}} \varphi_{\rho_{i+1}}^p V_{\beta_i\beta_{i+1}}^{\rho_{i+1}} \Phi_{p\beta_{i+1}}^{[i+2]}$, one-dot core tensor $C_{\beta_{i-1}\beta_i}^{\rho_i}$ can be optimized in the same way except for the SVD truncation. We observed that until the basis function Φ converged to the optimal value, the TT should be gradually optimized, but once basis function Φ converged, the TT optimization should be done by the CG method with tight convergence criteria. In addition, once the bond dimension M reaches the maximum value defined in advance, from the next sweeping, the optimization should be executed in the one-dot form $C_{\beta_{i-1}\beta_i}^{\rho_i}$, which is free from the truncation error. In general, increasing the bond dimension M enhances the representational power, but it also increases the risk of overfitting. Therefore, the bond dimension M is a crucial hyperparameter in TT optimization.

Algorithm 1 Conjugate gradient method for TT core optimization

$\Phi_{p\beta_{i-1}}^{[:i-1]} \in \mathbb{R}^{|\mathcal{D}'| \times M}$, $\Phi_{p\beta_{i+1}}^{[i+2:]} \in \mathbb{R}^{|\mathcal{D}'| \times M}$, $\varphi_{\rho_i}^p \in \mathbb{R}^{|\mathcal{D}'| \times N}$,
 $\varphi_{\rho_{i+1}}^p \in \mathbb{R}^{|\mathcal{D}'| \times N}$, $y_p \in \mathbb{R}^{|\mathcal{D}'|}$, $B, b, r_k, p_k \in \mathbb{R}^{M \times N \times N \times M}$

- 1: **function** GETAX($\Phi_{p\beta_{i-1}}^{[:i-1]}$, $\Phi_{p\beta_{i+1}}^{[i+2:]}$, $\varphi_{\rho_i}^p$, $\varphi_{\rho_{i+1}}^p$, $x_{\beta_{i-1}\beta_{i+1}}^{\rho_i\rho_{i+1}}$)
- 2: **return** $\sum_{p, \rho_i, \rho_{i+1}, \beta_{i-1}, \beta_{i+1}} \Phi_{p\beta_{i-1}}^{[:i-1]} \Phi_{p\beta_{i+1}}^{[i+2:]} \varphi_{\rho_i}^p \varphi_{\rho_{i+1}}^p \Phi_{p\beta_{i-1}}^{[:i-1]} \Phi_{p\beta_{i+1}}^{[i+2:]} \varphi_{\rho_i}^p \varphi_{\rho_{i+1}}^p x_{\beta_{i-1}\beta_{i+1}}^{\rho_i\rho_{i+1}}$
- 3: **end function**
- 1: **function** CONJUGATEGRADIENT($\Phi_{p\beta_{i-1}}^{[:i-1]}$, $\Phi_{p\beta_{i+1}}^{[i+2:]}$, $\varphi_{\rho_i}^p$, $\varphi_{\rho_{i+1}}^p$, y_p , $B_{\beta_{i-1}\beta_{i+1}}^{\rho_i\rho_{i+1}}$, k_{\max} , ϵ)
- 2: $B_0 \leftarrow B_{\beta_{i-1}\beta_{i+1}}^{\rho_i\rho_{i+1}}$
- 3: $b \leftarrow \sum_p \Phi_{p\beta_{i-1}}^{[:i-1]} \Phi_{p\beta_{i+1}}^{[i+2:]} \varphi_{\rho_i}^p \varphi_{\rho_{i+1}}^p y_p$
- 4: $r_0 \leftarrow b - \text{GetAx}(\Phi_{p\beta_{i-1}}^{[:i-1]}, \Phi_{p\beta_{i+1}}^{[i+2:]}, \varphi_{\rho_i}^p, \varphi_{\rho_{i+1}}^p, B_0)$
- 5: $p_0 \leftarrow r_0$
- 6: $k \leftarrow 0$
- 7: **while** $k < k_{\max}$ **do**
- 8: $Ap_k \leftarrow \text{GetAx}(\Phi_{p\beta_{i-1}}^{[:i-1]}, \Phi_{p\beta_{i+1}}^{[i+2:]}, \varphi_{\rho_i}^p, \varphi_{\rho_{i+1}}^p, p_k)$
- 9: $p_k^\top Ap_k \leftarrow \sum_{\rho_i, \rho_{i+1}} \sum_{\beta_{i-1}, \beta_{i+1}} (p_k)_{\beta_{i-1}\beta_{i+1}}^{\rho_i\rho_{i+1}} (Ap_k)_{\beta_{i-1}\beta_{i+1}}^{\rho_i\rho_{i+1}}$
- 10: $\alpha_k \leftarrow \frac{\|r_k\|^2}{p_k^\top Ap_k}$
- 11: $B_{k+1} \leftarrow B_k + \alpha_k p_k$
- 12: $r_{k+1} \leftarrow r_k - \alpha_k Ap_k$
- 13: **if** $\|r_{k+1}\| < \epsilon$ **then**
- 14: **break**
- 15: **end if**
- 16: $\beta_k \leftarrow \frac{\|r_{k+1}\|^2}{\|r_k\|^2}$
- 17: $p_{k+1} \leftarrow r_k + \beta_k p_k$
- 18: $k \leftarrow k + 1$
- 19: **end while**
- 20: **return** B_{k+1}
- 21: **end function**

C. Multi-dimensional integral

NN-MPO demonstrates sufficient capability as a high-precision energy predictor. However, its true strength lies in its compatibility with multi-dimensional integrals, such as the evaluation of expectation values. This section shows how the multi-dimensional integral between the wavefunction basis and the NN-MPO can be evaluated in polynomial time. We consider the wavefunction in f -dimensional space $\mathbf{q} \in \mathbb{R}^{1 \times f}$ written as

$$|\Psi\rangle = \sum_{\sigma} A_{\sigma} |\sigma_1(q_1)\rangle |\sigma_2(q_2)\rangle \cdots |\sigma_f(q_f)\rangle \quad (34)$$

where A_{σ} is the coefficient of each configuration σ . A_{σ} can be a linear combination of state vectors, mean-field wavefunction, or MPS.

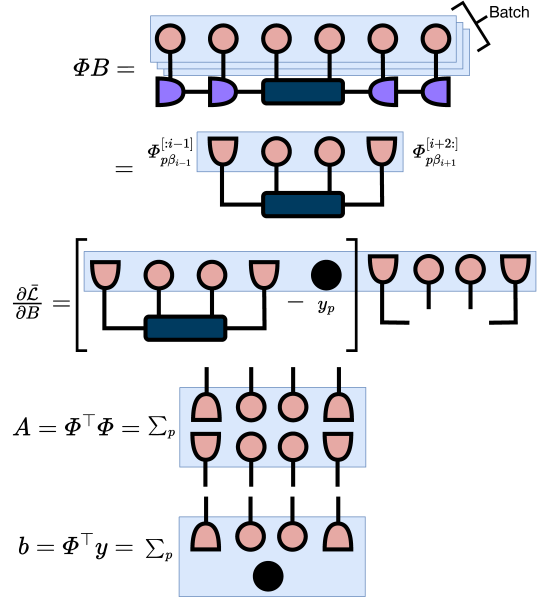


FIG. 5. The diagram of tensor network blocks used for the optimization.

We consider the Hamiltonian represented by

$$H = \sum_{i=1}^n -\frac{\hbar^2}{2} \frac{\partial^2}{\partial x_i^2} + V(x_1, x_2, \cdots, x_n) \quad (35)$$

$$\simeq \sum_{i=1}^f -\frac{\hbar^2}{2} \frac{\partial^2}{\partial q_i^2} + V(q_1, q_2, \cdots, q_f) \quad (36)$$

$$\simeq \sum_{i=1}^f -\frac{\hbar^2}{2} \frac{\partial^2}{\partial q_i^2} + \tilde{V}_{\text{NN-MPO}}(q_1, q_2, \cdots, q_f). \quad (37)$$

The first line, Eq (35), is the Hamiltonian in the mass-weighted coordinate space, in which atomic masses are absorbed into the positions x_i . The second line, Eq (36), is the Hamiltonian in the latent coordinate space \mathbf{q} , which is exact when $n = f$. Since the coordinate transformation is linear and orthogonal, the kinetic terms are kept in a simple form. The third line, Eq (37), is the Hamiltonian approximated by NN-MPO.

While the integral between kinetic terms and wavefunction is easily evaluated because it has a SOP form, the integral between the potential term and wavefunction is not trivial. To evaluate the integral, we need to prepare the potential operator \hat{V} , derived from inserting the projection operator

$$\hat{V} = \sum_{\sigma', \sigma} |\sigma'\rangle \langle \sigma' | \tilde{V}_{\text{NN-MPO}} | \sigma \rangle \langle \sigma | \quad (38)$$

where

$$|\sigma\rangle = |\sigma_1(q_1)\rangle |\sigma_2(q_2)\rangle \cdots |\sigma_f(q_f)\rangle. \quad (39)$$

At first, we evaluate one-dimensional integrals between

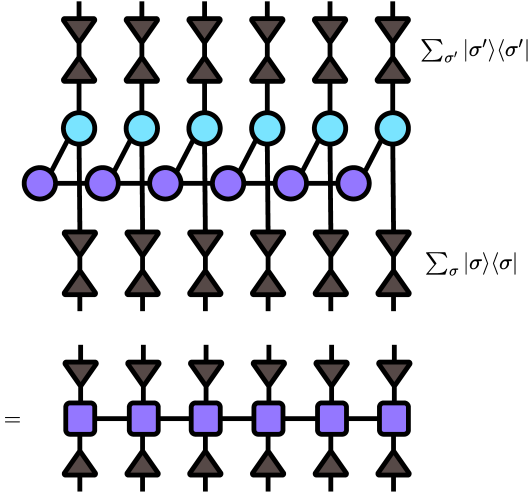


FIG. 6. Conversion process from NN-MPO to MPO.

potential basis $\phi_{\rho_i}(q_i)$ and wavefunction basis $\sigma_{j_i}(q_i)$:

$$I_{\rho_i \sigma_i}^{\sigma'_i} = \langle \sigma'_i(q_i) | \phi_{\rho_i}(q_i) | \sigma_i(q_i) \rangle. \quad (40)$$

The total cost of evaluating all $I_{\rho_i \sigma_i}^{\sigma'_i}$ is $\mathcal{O}(d^2 N f K)$, where d is the number of wavefunction basis, N is the number of potential basis, f is the degrees of freedom, and K is the cost of one-dimensional integral. Next, we contract TT-core tensor $W_{\beta_{i-1} \beta_i}^{\rho_i}$ and $I_{\rho_i \sigma_i}^{\sigma'_i}$:

$$\mathcal{W}_{\sigma_i \beta_i}^{\sigma'_i} = \sum_{\rho_i} W_{\beta_{i-1} \beta_i}^{\rho_i} I_{\rho_i \sigma_i}^{\sigma'_i}. \quad (41)$$

This contraction costs $\mathcal{O}(M^2 d^2 N f)$ where M is the bond dimension of TT. Finally, we have the MPO of the potential operator:

$$\hat{V} = \sum_{\sigma', \sigma} |\sigma'\rangle \sum_{\beta_1 \dots \beta_{f-1}} \mathcal{W}_{\beta_1 \beta_1}^{\sigma'_1} \mathcal{W}_{\beta_1 \beta_2}^{\sigma'_2} \dots \mathcal{W}_{\beta_{f-1} \beta_f}^{\sigma'_f} \langle \sigma |. \quad (42)$$

The conversion process is shown in Fig. 6.

By contracting from the left or right terminal site, the total evaluation cost of $\langle \sigma' | \hat{V} | \sigma \rangle$ reaches $\mathcal{O}(M^2 f)$ when wavefunction basis is orthogonal. The evaluation costs of mean-field operator $\langle \sigma^{(i')} | \hat{V} | \sigma^{(i)} \rangle$, where $|\sigma^{(i)}\rangle = |\sigma_1 \dots \sigma_{i-1} \sigma_{i+1} \dots \sigma_f\rangle$, is also $\mathcal{O}(M^2 f)$. As long as the wavefunction is represented by MPS or expanded by a polynomial number of configurations, the multi-dimensional integral can be evaluated in polynomial time.

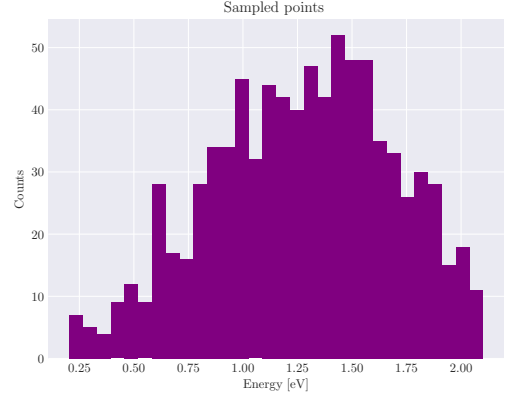


FIG. 7. Energy distribution of 839 test data points for H_2CO molecule. Energies are shifted by the energy at the equilibrium structure.

III. RESULTS AND DISCUSSION

A. Dataset sampling

To demonstrate the capability of the prediction and the compatibility with multi-dimensional integrals of NN-MPO, we show the application to 6-dimensional space spanned by all normal modes of formaldehyde H_2CO as a test case. H_2CO is a typical benchmark molecule for both full-quantum approach and machine learning potential [23, 45–47] due to its strong anharmonicity and many-body correlation. In this work, the input to the model is a position represented by six normal coordinates, and the output is a ground state energy at that position. Energies and forces were computed by density functional theory (DFT) with the B3LYP functional and the SVP basis set with JK-fit approximation implemented in the BAGEL program package [48]. Samplings were performed from inverted potential probability density function [49]

$$P(V) \propto \max\left(\frac{V_{\max} + \Delta - V}{V_{\max} + \Delta}, 0\right) \quad (43)$$

where we set $V_{\max} = 17,000 \text{ cm}^{-1}$ and $\Delta = 500 \text{ cm}^{-1}$, which are the same values as previous work [45]. From this distribution, in this work, 625 training data points and DFT energies up to V_{\max} were sampled by Metropolis-Hastings algorithm while previous work used analytical SOP model potential [50] spanned by six internal coordinates and sampled by *quasi* Monte Carlo method in the hypercube [45]. We should note that any SOP model potential can be exactly encoded into NN-MPO by choosing the appropriate basis in the same way as general MPO does [51, 52]. The sampled test data are shown in Fig. 7.

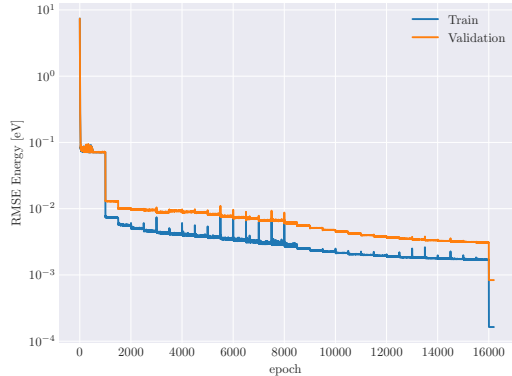


FIG. 8. Training trace of the NN-MPO for H_2CO molecule. For the first 1,000 epochs, basis and TT were optimized iteratively in short epochs. During 1,000-16,000 epochs, sweeping was executed every 500 epochs. Final drastic convergence was achieved by sweeping using the CG method.

B. Training results

We set the input dimension as $n = 6$, the latent dimension as $f = 6$, the number of basis as $N = 21$, the bond dimension as $M = 2$ for the initial state, and $M = 14$ for the maximum. The order of the input normal coordinates was assigned in the harmonic oscillator (HO) frequency order. The training trace is shown in Fig. 8. For the basis optimization, we divided the 625 training points into five mini-batches, each containing 125 points. For the first 1,000 epochs, to make a good initial guess, one-dot sweeping and basis optimization by Adam were performed iteratively and confirmed the loss function was roughly converged. From 1,000 epochs to 16,000 epochs, to increase a representational power, two-dot sweeping was executed every 500 epochs and switched to one-dot sweeping once the bond dimension reached 14. Finally, we fixed the basis and refined TT by one-dot sweeping using the CG method until it tightly converged. The final root mean square error (RMSE) of the energy for the validation set reached less than 1.0 meV. The scatter plot between the predicted and test energy is shown in Fig. 9 and the mean absolute error (MAE) was 3.03 cm^{-1} . Fig. 10 shows the matrix elements of the coordinator U of the NN-MPO after training, which indicates that initial normal modes are suitable for the description of the PES in a low-rank tensor network because the coordinator matrix is almost the identity matrix. If we examine the coordinator matrix further, we see that the x_3 and x_4 are slightly mixed. This should be because both have the same symmetry, A_1 irreducible representation, and close harmonic frequencies around $1,500$ to $1,800 \text{ cm}^{-1}$. The displacement vector of q_4 (C=O stretching) is a little bit different from x_4 in terms of the $\angle\text{H}_1\text{OH}_2$ angle. The x_1 , unique out-of-plane mode, is the most separated from the others. In the present results, significant rotations of the

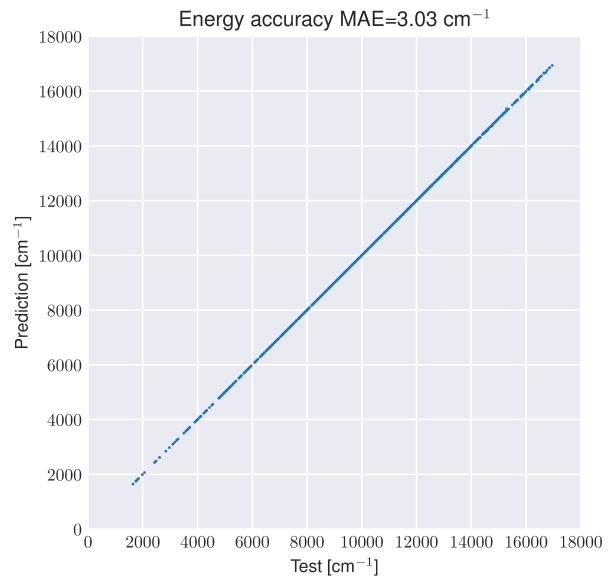


FIG. 9. Scatter plot of the predicted and test energy for H_2CO molecule.

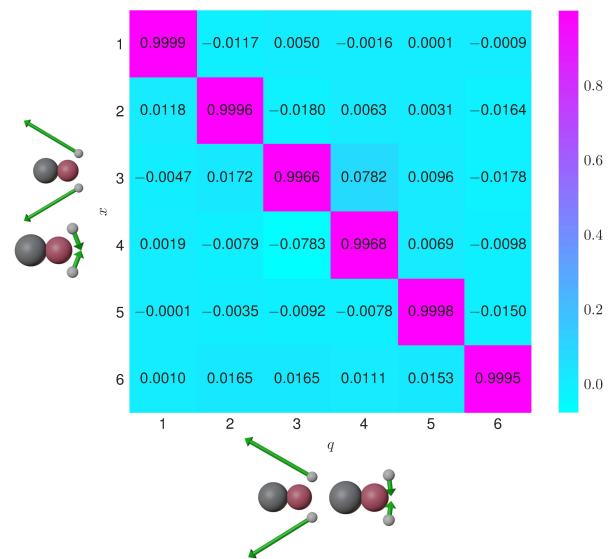


FIG. 10. Coordinator U of NN-MPO for the normal modes of H_2CO molecule. Row and column indices are the initial normal modes x and the latent modes q , respectively.

coordinate were not observed. However, we initially had anticipated that similar to how diagonalizing the Hessian matrix provides the coordinates that yield the lowest-rank, TT-rank 2, structure in the HO approximation, training the coordinator within the manifold of low-rank approximations of realistic potentials would also yield advantageous coordinates. For further details, including hyperparameters, we provide our NN-MPO implementation at <https://github.com/KenHino/Pompon>.

C. DMRG calculations

After NN-MPO had been trained, we solved the Schrödinger equation, Eq. (37), to obtain the first 21 vibrational levels of the H_2CO molecule. We chose wavefunction basis $|\sigma_i\rangle$ as HO discrete variable representation (DVR) [17, 53], which is derived from the diagonalization of the representation matrix between HO eigenfunctions and position operator, and enables us to approximate the integral between position-dependent function and DVR basis by evaluating the function value at DVR grid points. We used our DVR basis implementation available at <https://github.com/KenHino/Discvar>. DVR grid basis $|n\rangle$ has been facilitated by MPS and MPO framework [54]. Both the kinetic operator and NN-MPO were converted to MPO, and phonon DMRG calculation was performed by using `ITensors.jl` library version 0.6 available at <https://github.com/ITensor/ITensors.jl> [55]. Kinetic MPO is given by $M = 2$;

$$-\frac{\hbar^2}{2} [\hat{p}_1^2 \ 1] \begin{bmatrix} 1 & 0 \\ \hat{p}_2^2 & 1 \end{bmatrix} \cdots \begin{bmatrix} 1 & 0 \\ \hat{p}_{f-1}^2 & 1 \end{bmatrix} \begin{bmatrix} 1 \\ \hat{p}_f^2 \end{bmatrix} \quad (44)$$

where \hat{p}_i is the momentum operator of i -th basis. We set the number of wavefunction basis $d = 9$ and the maximum bond dimension of MPS $m = 100$. The vibrational levels calculated by NN-MPO are shown in Fig 11 and compared with HO approximation and the full-dimensional mesh grid potential (exact MPO), which requires DFT calculations for all possible $d^6 = 531,441$ DVR grid points and reaches its bond dimension to $M = d^3 = 729$ without any compression. The MAE of twenty excited vibrational levels between NN-MPO and exact MPO was 0.318 cm^{-1} . The large deviation of ZPE about 40 cm^{-1} might be attributed to the difference between coordinates spanning Hilbert space and the lack of sampling points around the equilibrium geometry, as shown in Fig 7. As the dimension increases, sampling around the equilibrium geometry becomes more challenging due to its decreasing relative volume. However, importance sampling can provide a solution to this problem.

IV. CONCLUSIONS

We have introduced the neural network matrix product operator (NN-MPO), which can be trained with energy and force at randomly sampled points and is compatible with multi-dimensional integral. We have successfully applied a six-dimensional system to demonstrate that the NN-MPO can predict DFT energies with MAE of 3.03 cm^{-1} , where the energies reach up to $17,000 \text{ cm}^{-1}$, using only 625 training data points. In addition, we have introduced the coordinator U as a trainable parameter, orthogonal linear transformation matrix from the input mass-weighted coordinates \mathbf{x} , which would yield a suit-

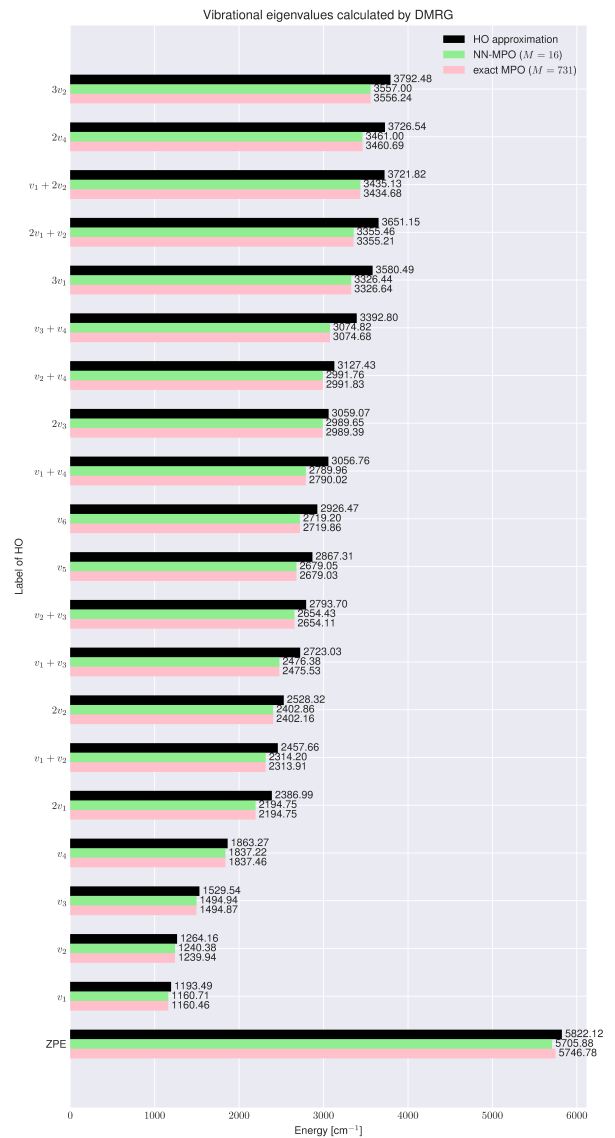


FIG. 11. Vibrational eigenvalues of the H_2CO molecule calculated by HO approximation and DMRG using NN-MPO and exact MPO.

able coordinate for quantum mechanics calculations because the kinetic energy operator is kept the simple form and the latent coordinate leads to a lower-rank representation. Using trained NN-MPO, we performed the phonon DMRG calculation and MAE of the vibrational excited levels between NN-MPO and exact MPO, reaching a spectroscopic accuracy of 0.318 cm^{-1} . However, several challenges remain. For instance, the symmetry of the molecule should be considered, which not only enhances the sampling efficiency but also avoids unphysical predictions such as lifted degeneracy of the energy levels. The proper coordinate can introduce translational and rotational invariance, although sophisticated internal coordinates, such as poly-spherical coordinates, tend to complicate the kinetic energy operator. The adoption of the permutational invariance is not straightfor-

ward. The permutationally invariant polynomial (PIP) [47, 56–58] may give us a hint on how to address this issue. The quantum number conservation approach, which is used for electronic MPS wavefunction, may enhance the capability of the NN-MPO. Furthermore, the scalability involving the number of parameters, training data points, and optimization convergence has not yet been explored. Ideally, NN-MPO can express PES with a scalable number of parameters if the system involves short-range interactions, such as hydrogen bonds or Van der Waals interactions, or exhibits a one-dimensional structure, like polyenes. The CG method is a robust approach to solving quadratic optimization problems; however, it becomes challenging when the number of data points $|\mathcal{D}|$ is enormous, particularly as the system size increases. *Novikov et al* have proposed a different optimization scheme for TT [59] facilitated by the Riemannian optimization, which is oriented to mini-batch optimization. The NN-MPO can be applied not only to MPS wavefunctions but also to a linear combination of state vectors and mean-field wavefunctions. In contrast, the SOP is typically employed for a wide range of tensor networks, including tree tensor networks like the multi-layer MCTDH

[60]. Despite these issues, our method offers a promising alternative for quantum many-body simulations. It bridges the gap between traditional SOP representations and modern machine learning techniques and allows us to approach the Born-Oppenheimer approximation limit accurately. Moreover, multi-dimensional integrals arise in various contexts, such as evaluating expectation values, variational optimization, marginalizing degrees of freedom, and calculating free energy using configuration integrals. By harnessing the capabilities of the NN-MPO for these applications, we can position it as a versatile instrument not only within quantum mechanics but across a broader spectrum of scientific disciplines.

ACKNOWLEDGMENTS

This work was supported by JSPS KAKENHI (JP23KJ1334, JP23H01921), JST-FOREST Program (JPMJFR221R), JST-CREST Program (JPMJCR23I6), and MEXT Q-LEAP Program (JPMXS0120319794).

-
- [1] J. Behler, *Phys. Chem. Chem. Phys.* **13**, 17930 (2011).
 [2] J. Behler, *International Journal of Quantum Chemistry* **115**, 1032 (2013).
 [3] J. Behler, *The Journal of Chemical Physics* **145**, 170901 (2016).
 [4] K. Schütt, P.-J. Kindermans, H. E. Saucedo Felix, S. Chmiela, A. Tkatchenko, and K.-R. Müller, in *Advances in Neural Information Processing Systems*, Vol. 30 (Curran Associates, Inc., 2017).
 [5] V. L. Deringer, M. A. Caro, and G. Csányi, *Advanced Materials* **31**, 1902765 (2019).
 [6] S. Takamoto, C. Shinagawa, D. Motoki, K. Nakago, W. Li, I. Kurata, T. Watanabe, Y. Yayama, H. Iriguchi, Y. Asano, T. Onodera, T. Ishii, T. Kudo, H. Ono, R. Sawada, R. Ishitani, M. Ong, T. Yamaguchi, T. Kataoka, A. Hayashi, N. Charoenphakdee, and T. Ibuka, *Nat Commun* **13**, 2991 (2022).
 [7] J. Behler, *The Journal of Chemical Physics* **134**, 074106 (2011).
 [8] O. T. Unke and M. Meuwly, *J. Chem. Theory Comput.* **15**, 3678 (2019).
 [9] S. Batzner, A. Musaelian, L. Sun, M. Geiger, J. P. Mailoa, M. Kornbluth, N. Molinari, T. E. Smidt, and B. Kozinsky, *Nat Commun* **13**, 2453 (2022).
 [10] I. Batatia, D. P. Kovacs, G. Simm, C. Ortner, and G. Csanyi, *Advances in Neural Information Processing Systems* **35**, 11423 (2022).
 [11] S. Takamoto, S. Izumi, and J. Li, *Computational Materials Science* **207**, 111280 (2022).
 [12] C. Zhang, S. Bengio, M. Hardt, B. Recht, and O. Vinyals, *Commun. ACM* **64**, 107 (2021).
 [13] J. Frankle and M. Carbin, *The Lottery Ticket Hypothesis: Finding Sparse, Trainable Neural Networks*, *Phys. Rev. Lett.* **69**, 2863 (1992). (2019), arXiv:1803.03635.
 [14] Z. Allen-Zhu, Y. Li, and Z. Song, in *Proceedings of the 36th International Conference on Machine Learning* (PMLR, 2019) pp. 242–252.
 [15] L. Zhang, J. Han, H. Wang, R. Car, and W. E, *Phys. Rev. Lett.* **120**, 143001 (2018).
 [16] H. Wang, L. Zhang, J. Han, and W. E, *Computer Physics Communications* **228**, 178 (2018).
 [17] M. H. Beck, A. Jäckle, G. A. Worth, and H. D. Meyer, *Phys. Rep.* **324**, 1 (2000).
 [18] H. D. Meyer, U. Manthe, and L. S. Cederbaum, *Chemical Physics Letters* **165**, 73 (1990).
 [19] A. Jäckle and H.-D. Meyer, *The Journal of Chemical Physics* **104**, 7974 (1996).
 [20] R. L. Panadés-Barrueta and D. Peláez, *The Journal of Chemical Physics* **153**, 234110 (2020).
 [21] M. Schröder, *The Journal of Chemical Physics* **152**, 024108 (2020).
 [22] Q. Song, X. Zhang, D. Peláez, and Q. Meng, *J. Phys. Chem. Lett.* **13**, 11128 (2022).
 [23] W. Koch, M. Bonfanti, P. Eisenbrandt, A. Nandi, B. Fu, J. Bowman, D. Tannor, and I. Burghardt, *The Journal of Chemical Physics* **151**, 064121 (2019).
 [24] S. Manzhos and T. Carrington, Jr., *The Journal of Chemical Physics* **125**, 194105 (2006).
 [25] N. Nadoveza, R. L. Panadés-Barrueta, L. Shi, F. Gatti, and D. Peláez, *The Journal of Chemical Physics* **158**, 114109 (2023).
 [26] S. Sasmal, M. Schröder, and O. Vendrell, *The Journal of Chemical Physics* **160**, 064109 (2024).
 [27] G. Li, C. Rosenthal, and H. Rabitz, *J. Phys. Chem. A* **105**, 7765 (2001).
 [28] S. Manzhos and T. Carrington, *The Journal of Chemical Physics* **125**, 084109 (2006).
 [29] S. R. White, *Phys. Rev. Lett.* **69**, 2863 (1992).
 [30] S. R. White, *Phys. Rev. B* **48**, 10345 (1993).
 [31] G. K.-L. Chan and M. Head-Gordon, *The Journal of Chemical Physics* **116**, 4462 (2002).

- [32] G. K.-L. Chan and S. Sharma, *Annual Review of Physical Chemistry* **62**, 465 (2011).
- [33] A. Baiardi, C. J. Stein, V. Barone, and M. Reiher, *J. Chem. Theory Comput.* **13**, 3764 (2017).
- [34] E. Stoudenmire and D. J. Schwab, in *Advances in Neural Information Processing Systems*, Vol. 29 (Curran Associates, Inc., 2016).
- [35] B. Pirvu, V. Murg, J. I. Cirac, and F. Verstraete, *New J. Phys.* **12**, 025012 (2010).
- [36] V. Baranov and I. Oseledets, *The Journal of Chemical Physics* **143**, 174107 (2015).
- [37] I. Oseledets and E. Tyrtyshnikov, *Linear Algebra and its Applications* **432**, 70 (2010).
- [38] I. V. Oseledets, *SIAM J. Sci. Comput.* **33**, 2295 (2011).
- [39] P. Ramachandran, B. Zoph, and Q. V. Le, *Searching for Activation Functions* (2017), arXiv:1710.05941 [cs].
- [40] J. Bradbury, R. Frostig, P. Hawkins, M. J. Johnson, C. Leary, D. Maclaurin, G. Necula, A. Paszke, J. VanderPlas, S. Wanderman-Milne, and Q. Zhang, *JAX: composable transformations of Python+NumPy programs* (2018).
- [41] D. P. Kingma and J. Ba, *Adam: A Method for Stochastic Optimization* (2017), arXiv:1412.6980 [cs].
- [42] S. Bonnabel, *IEEE Transactions on Automatic Control* **58**, 2577 (2013).
- [43] G. Bécigneul and O.-E. Ganea, *Riemannian Adaptive Optimization Methods* (2019), arXiv:1810.00760 [cs, stat].
- [44] M. Kochurov, R. Karimov, and S. Kozlukov, *Geopt: Riemannian optimization in pytorch* (2020), arXiv:2005.02819 [cs.CG].
- [45] A. Kamath, R. A. Vargas-Hernández, R. V. Kreams, T. Carrington, and S. Manzhos, *The Journal of Chemical Physics* **148**, 241702 (2018).
- [46] S. Manzhos and T. J. Carrington, *Chem. Rev.* **121**, 10187 (2021).
- [47] D. Koner and M. Meuwly, *J. Chem. Theory Comput.* **16**, 5474 (2020).
- [48] T. Shiozaki, *Wiley Interdiscip. Rev.: Comput. Mol. Sci.* **8**, 10.1002/wcms.1331 (2018).
- [49] J. Ku, A. Kamath, T. J. Carrington, and S. Manzhos, *J. Phys. Chem. A* **123**, 10631 (2019).
- [50] B. S. C. N. C. HANDY and JEAN. DEMAISON, *Molecular Physics* **90**, 729 (1997).
- [51] J. Ren, W. Li, T. Jiang, and Z. Shuai, *J. Chem. Phys.* **153**, 084118 (2020).
- [52] G. M. Crosswhite and D. Bacon, *Phys. Rev. A* **78**, 012356 (2008).
- [53] D. T. Colbert and W. H. Miller, *J. Chem. Phys.* **96**, 1982 (1992).
- [54] K. Hino and Y. Kurashige, *J. Chem. Theory Comput.* **20**, 3839 (2024).
- [55] M. Fishman, S. White, and E. M. Stoudenmire, *SciPost Physics Codebases*, 004 (2022).
- [56] B. J. Braams and J. M. Bowman, *International Reviews in Physical Chemistry* **28**, 577 (2009).
- [57] B. Jiang and H. Guo, *The Journal of Chemical Physics* **139**, 054112 (2013).
- [58] B. Jiang, J. Li, and H. Guo, *International Reviews in Physical Chemistry* **35**, 479 (2016).
- [59] A. Novikov, M. Trofimov, and I. Oseledets, *Exponential Machines* (2017), arXiv:1605.03795 [cs, stat].
- [60] H. Wang and M. Thoss, *J. Chem. Phys.* **119**, 1289 (2003).